

1
2
3
4 **Surface Loading Effects on Orthophosphate Surface Complexation at the**
5
6
7 **Goethite/Water Interface as Examined by Extended X-Ray Absorption Fine**
8
9 **Structure (EXAFS) Spectroscopy**
10

11
12
13
14 ABDALA, Dalton Belchior ¹, NORTHRUP, Paul Andrew ², ARAI, Yuji ³,
15
16 SPARKS, Donald Lewis ⁴
17
18
19
20

21 ¹Abdala, Dalton Belchior – Ph.D. graduate student, Plant & Soil Sciences
22
23 department, University of Delaware, Newark, DE – 19716, United States of America
24
25
26

27
28 ²Northrup, Paul Andrew – Senior Research Scientist, Stony Brook University,
29
30 National Synchrotron Light Source, Brookhaven National Laboratory, Upton, NY –
31
32 11973 – United States of America
33
34
35

36
37
38 ³Arai, Yuji – Assistant Professor, Department of Natural Resources and
39
40 Environmental Sciences, University of Illinois at Urbana-Champaign, Urbana, IL –
41
42 61801, United States of America
43
44
45

46
47
48 ⁴Sparks, Donald Lewis – S. Hallock du Pont Chair, Department of Plant & Soil
49
50 Sciences and Delaware Environmental Institute, University of Delaware, Newark, DE –
51
52 19716, United States of America
53
54
55

1
2
3
4
5
6
7
8
9
10
11
12
13
14
15
16
17
18
19
20
21
22
23
24
25
26
27
28
29
30
31
32
33
34
35
36
37
38
39
40
41
42
43
44
45
46
47
48
49
50
51
52
53
54
55
56
57
58
59
60
61
62
63
64
65

* Corresponding author: Dalton Belchior Abdala, telephone: (Brazil) +55 19 8354
6682, daltonabdala@gmail.com , Brazilian Synchrotron Light Laboratory. Rua Giuseppe
Maximo Scolfaro, 10 000 – Campinas, ZIP 13 083-970, SP – Brazil

1
2
3
4 **Abstract**
5
6
7
8

9 To investigate the effect of P surface loading on the structure of surface complexes
10 formed at the goethite/water interface, goethite was reacted with orthophosphate at P
11 concentrations of 0.1, 0.2, and 0.8 mmol L⁻¹ at pH 4.5 for 5 days. The P concentrations
12 were chosen to ensure that P loadings at the surface would allow one to follow the
13 transition between adsorption and surface precipitation. Extended X-ray Absorption Fine
14 Structure (EXAFS) spectra were collected in fluorescence mode at the P K-edge at 2,150
15 eV. The structural parameters were obtained through the fits of the sorption data to single
16 and multiple scattering paths using Artemis. EXAFS analysis revealed a continuum
17 among the different surface complexes, with bidentate mononuclear (²E), bidentate
18 binuclear (²C) and monodentate mononuclear (¹V) surface complexes forming at the
19 goethite/water interface under the studied conditions. The distances for P – O (1.51 – 1.53
20 Å) and P – Fe (3.2 – 3.3 Å for bidentate binuclear and around 3.6 Å for mononuclear
21 surface complexes) shells observed in our study were consistent with distances obtained
22 via other spectroscopic techniques. The shortest P – Fe distance of 2.83 – 2.87 Å was
23 indicative of a bidentate mononuclear bonding configuration. The coexistence of different
24 surface complexes or the predominance of one sorption mechanism over others was
25 directly related to surface loading.
26
27
28
29
30
31
32
33
34
35
36
37
38
39
40
41
42
43
44
45
46
47
48
49
50
51
52

53 **Keywords:** phosphorus solid-state speciation, phosphorus surface complexation,
54 phosphorus K-edge EXAFS, phosphorus retention mechanisms.
55
56
57
58
59
60
61
62
63
64
65

1
2
3
4 **1. INTRODUCTION**
5
6
7
8

9 The combination of strong binding of phosphorus (P) in soils, leading to its limited
10 availability to plants, particularly, in highly weathered soils of the tropics, and the
11 dependence of agriculture upon such soils for food production has motivated researchers
12 to examine the sorption mechanisms of P in soils and soil components. From an
13 environmental standpoint, issues surrounding excess P, often due to the disposal of P-rich
14 agricultural byproducts to agricultural lands, have also prompted researchers to address
15 the chemical reactions controlling the reactivity and transport of this element ¹⁻⁵.
16
17
18
19
20
21
22
23
24
25

26 The adsorption phenomenon involving oxyanions and soil mineral oxides was
27 originally thought to be characterized by an exchange reaction, which took place on the
28 surface of soil minerals like Fe and Al (hydr)oxides. Early investigations aimed at
29 understanding P bioavailability observed that phosphate exhibited some hysteresis and
30 that behavior was attributed to the formation of more thermodynamically stable
31 quasicomplexes or surface complexes. Elucidation of the surface complexes was
32 speculative and inferred from multiple linear portions of the Langmuir plot, which were
33 attributed to sites of varying reactivity ^{6, 7}. Hingston et al. ⁸⁻¹¹ studied the sorption of
34 several oxyanions, including P, As and S, on goethite and gibbsite and concluded that the
35 elemental selectivity of sorption was indeed due to specific sorption. It was only with the
36 help of molecular-scale techniques that the lack of molecular descriptions of the surface
37 complexes was fulfilled, bonding configurations corresponding to the different sorption
38 mechanisms were first observed and chemisorption reactions were shown to be involved
39
40
41
42
43
44
45
46
47
48
49
50
51
52
53
54
55
56
57
58
59
60
61
62
63
64
65

1
2
3
4 Over the past decades, solid-phase speciation studies of P have relied largely on the
5 use of spectroscopic techniques, especially Fourier transform infra-red (FTIR)^{13–18} and
6 Nuclear Magnetic Resonance (NMR)^{19–23} spectroscopies. A number of studies have
7 been conducted to elucidate the sorption mechanisms and surface
8 complexation/precipitation dependence on environmental conditions, particularly pH and
9 P loading. Overall, and regardless of the technique employed, there seems to exist a
10 consensus that the possible bonding configurations between phosphate and Fe and Al
11 (hydr)oxides include bidentate binuclear (²C) and monodentate mononuclear (¹V)
12 structures (Table 1). Nevertheless, interpretations of surface complex structures, such as
13 whether monodentate or bidentate complexes form, and the conditions at which they form
14 are not clear. In terms of goethite, Infrared (IR) studies have suggested that an inner-
15 sphere bidentate binuclear surface complex may be the predominant mechanism at low
16 pHs^{13,17} and low surface loading²³. Kwon & Kubicki²⁴ employed MO/DFT calculations
17 to model surface complexes and their findings corroborate the above studies. In a novel
18 study employing NMR to address P sorption to Fe (hydr)oxides, Kim et al.²² studied the
19 bonding mechanisms of P over a wide range of P concentration (0.1 – 3 mM) and pH (3 –
20 11) that encompasses most of the previous studies. They observed that a bidentate
21 binuclear complex was formed regardless of environmental conditions. However, a
22 monodentate mononuclear surface complex has also been suggested at low pHs¹⁴ and at
23 high P loadings²³. IR studies on other Fe (hydr)oxides include the work on ferrihydrite
24 by Arai & Sparks¹⁵, in which the authors have suggested that bidentate binuclear surface
25 complexes that formed at pH 4 to 6 were protonated and unprotonated complexes formed
26 at pH ≥ 7.5. Elzinga & Sparks¹⁶, working with hematite, observed the formation of
27
28
29
30
31
32
33
34
35
36
37
38
39
40
41
42
43
44
45
46
47
48
49
50
51
52
53
54
55
56
57
58
59
60
61
62
63
64
65

1
2
3
4 bidentate binuclear structures at lower pHs and higher surface loadings in the 3.5–7.0 pH
5
6 range whereas, at the highest pH values studied (8.5–9.0), a monodentate mononuclear
7
8 complex was present and its importance increased with increasing surface coverage at
9
10 high pH values. It is worth pointing out that the controversies surrounding the accurate
11
12 determination of sorption mechanisms are due to the lack of direct evidence together with
13
14 the reliance of the molecular assignments on an analytical approach ^{25, 26}. An additional
15
16 aspect that most of the early studies fail to precisely address is the formation of surface
17
18 precipitates ¹⁵ i.e., three dimensional entities formed when further increases in sorbate
19
20 concentration exceeds a monolayer coverage on the mineral surface. A vast literature on
21
22 this topic indicates that surface loading has a pronounced effect on the continuum
23
24 between surface complexation and surface precipitation on a number of soil minerals and
25
26 environmentally important elements ^{27–33}. At high P concentrations, surface precipitation
27
28 may be catalyzed leading to a new solid phase that is less readily dissolved or desorbed.
29
30 According to Sparks ³⁴, surface complexation tends to dominate at low surface coverages.
31
32 As surface coverage increases, nucleation is operational and results in the formation of
33
34 distinct entities or aggregates on the surface. As surface loadings increase further, surface
35
36 precipitation becomes the dominant mechanism.
37
38
39
40
41
42
43
44

45
46 Synchrotron-based X-ray absorption spectroscopy (XAS) has been extensively
47
48 applied to model systems to resolve molecular-level sorption mechanisms of a number of
49
50 soil contaminants ^{15, 35, 36}. These tools can greatly improve our understanding of P
51
52 reactions in soils and provide predictions on an atomic/molecular basis of mechanisms of
53
54 P retention on soil minerals. Such data are useful in the development of molecular
55
56 sorption models if one aims to relate P speciation to P mobilization. Whereas the use of
57
58
59
60
61
62
63
64
65

1
2
3
4 state-of-the-art techniques, such as XAS (XANES and EXAFS) can enhance our
5
6 knowledge on the reaction processes that elements undergo in the environment, some
7
8 limitations may constrain their widespread use. When it comes to EXAFS analysis of
9
10 low-Z elements such as P, fluorescence yield decreases with decreasing atomic number,
11
12 which is reflected in the poor signal:noise. This ultimately hinders the collection of high
13
14 quality data. In addition, in dilute samples, e. g., environmental samples, fluorescence
15
16 attenuation is severely augmented especially in a dense, high-Z matrix such as goethite.
17
18
19
20

21 It is noteworthy to mention that ³⁷⁻³⁹ employed XANES to distinguish P adsorption
22
23 from surface precipitation at mineral/water interfaces. However, in their studies, the
24
25 authors relied on indirect observations to address the bonding configurations of the
26
27 surface structures being formed on the mineral surface, namely, the full width at half
28
29 maximum height (FWHM) concept and extended Hückel calculations. Therefore, to the
30
31 best of our knowledge, our study is the first to employ EXAFS to collect direct
32
33 information on the P sorption mechanisms formed at the mineral/water interface.
34
35
36
37

38 Accordingly, we combined a batch technique with EXAFS spectroscopy to
39
40 examine the effects of surface loading and pH on the local atomic environment of sorbed
41
42 P at the goethite/water interface.
43
44
45
46
47

48 **2. MATERIAL & METHODS**

49
50
51
52

53 *2.1 Mineral Synthesis*

54
55

56 Goethite was synthesized according to the method of Schwertmann & Cornell ⁴⁰.
57
58 Briefly, 200 mL of 1 M Fe(NO₃)₃ · 9 H₂O were added to a plastic flask with continuous
59
60
61
62
63
64
65

1
2
3
4 stirring and then 360 mL of 5 M KOH were carefully added. Four L of DDI water were
5
6 added and the mixture was thoroughly mixed for 30 min. The flask was sealed with
7
8 Scotch duct tape and placed in an oven set at 70 °C for 4 days. After the 4th day, the
9
10 supernatant solution was poured off and the goethite precipitate, which had settled to the
11
12 bottom of the container, was washed with dialysis tubing for about one week until the
13
14 electric conductivity matched that of the distilled deionized water ($\sim 0.95 \mu\text{S cm}^{-1}$). The
15
16 dialyzed mineral was transferred into 50 mL centrifuge tubes and centrifuged at 11 000
17
18 rpm for 30 min. The supernatant was removed with a syringe and the precipitate was
19
20 freeze dried for approximately 60 h. Finally, the material was softly ground in a mortar
21
22 and stored in a polystyrene bottle.
23
24
25
26
27

28
29 The specific surface area of the goethite, determined by a three point Brunauer-
30
31 Emmett-Teller N₂ gas adsorption isotherm, was $40.0 \pm 0.6 \text{ m}^2 \text{ g}^{-1}$.
32
33
34
35

36 2.2 Sorption Experiments

37

38
39 Centrifuge tubes containing stock goethite suspensions of 20 g L^{-1} were placed in a
40
41 rotating shaker set at 30 rpm at 298 K and equilibrated in 50 mmol L^{-1} KCl with the pH
42
43 adjusted to 4.5 for 36 h prior to phosphate addition. The pH in the suspensions was
44
45 monitored throughout the shaking period and adjusted to the target pH as needed by the
46
47 addition of either NaOH or HCl. Thereafter, an aliquot of the suspension was transferred
48
49 to a new centrifuge tube to yield a goethite suspension of 2 g L^{-1} , and a phosphate
50
51 solution of 0.1, 0.2, and 0.8 mmol L^{-1} was added. This corresponded to surface coverages
52
53 of 1.25, 2.5 and $10 \mu\text{mol m}^{-2}$. The tubes were shaken and 5 mL aliquots from each tube
54
55 were sampled on the 5th day.
56
57
58
59
60
61
62
63
64
65

1
2
3
4 The phosphate concentrations were carefully chosen to ensure a range of surface
5 coverages. The reaction time, 5 days, was shown to be sufficient to ensure that the bulk of
6 the added P (> 95%) was associated with the surface.
7
8
9

10 11 12 13 14 2.3 XAS Sample Preparation and Analysis 15

16 Each sample was immediately filtered to pass through a 0.22 μm nitrocellulose
17 membrane filter and washed three times with 3 mL of pH adjusted 50 mmol L^{-1} KCl to
18 remove any entrained phosphate not associated with the surface. The cellulose membrane
19 filter containing the mineral paste was sealed with 5-micron polypropylene XRF thin film
20 (Ultralene®) and stored moist in a sealed sample box at 6 °C until analysis. The samples
21 were stored for no more than 24 h prior to analysis. Phosphorus K-edge spectra (2,150
22 eV) were collected at beamline X15B at the National Synchrotron Light Source (NSLS)
23 at Brookhaven National Laboratory. The X15B sample chamber is a “hutch box”
24 containing a He atmosphere at 1.001 atm positive pressure.
25
26
27
28
29
30
31
32
33
34
35
36
37

38 EXAFS spectra were collected in fluorescence mode with samples mounted at 45°
39 to the incident beam, using a liquid-nitrogen-cooled Canberra Ultra-Low-Energy
40 Germanium detector positioned at 90°. X15B beamline optics consist of a collimating
41 and harmonic-rejection mirror, a monochromator utilizing Si (111) crystals to tune
42 energy, and a focusing mirror to gather approximately 5×10^{11} photons sec^{-1} into a 1-mm
43 spot at the sample position. The fluorescence signal was normalized to incident beam
44 intensity as measured using a windowless ionization chamber. XAS spectra were
45 collected at photon energies between 2099 and 2750 eV with a minimum step size of 0.1
46 eV across the edge and gradually increasing step sizes up to 6 eV at 2750 eV. The
47
48
49
50
51
52
53
54
55
56
57
58
59
60
61
62
63
64
65

1
2
3
4 collected spectra were processed using the Athena software in the computer package
5
6 IFEFFIT⁴¹. Six to ten individual spectra were averaged for each sample.
7
8
9

10 11 *2.3.1 EXAFS Data Analysis* 12 13

14 The averaged spectra were normalized to an atomic absorption of one, and the
15
16 EXAFS signal was extracted from the raw data using linear pre-edge and a quadratic
17
18 spline post-edge, followed by subtraction of background using the Autobk algorithm⁴².
19
20 Data were converted from energy to photo electron momentum (k-space) and k-weighted
21
22 by k^2 . Fourier transforms (FT) of the k^2 -weighted EXAFS were calculated over a k-range
23
24 of 2.0 to between 10.1 and 10.6 to obtain the R-space. The FT of the EXAFS was fit with
25
26 the predicted neighbor paths by varying the number of coordinating atoms (CN), their
27
28 distance (ΔR), mean square displacement (δ^2) and passive electron reduction factor (S_0^2)
29
30 in order to obtain the best fit between the experimental and predicted spectra.
31
32
33
34
35

36 First shell (P – O) bond distances were obtained from the literature from
37
38 crystallographic data and were used in the fit and fixed at these values for higher shell
39
40 fitting. We fixed the CN of the first oxygen shell at 4 as the regular coordination
41
42 environment of PO_4 ions. Fits to second neighbor Fe shells were made by setting the
43
44 degeneracy of each surface complex, CN = 2 for bidentate binuclear or CN = 1 for either
45
46 bidentate mononuclear or mononuclear coordination, and fitting an amplitude factor
47
48 describing the fraction of P in each configuration. One may argue about the method used
49
50 to fit first and second coordination shells, that is, by setting the CN instead of floating it,
51
52 as is standard practice. Indeed, floating CN was our first approach. However, the misfit
53
54 between data and fit was large enough to consider the approach we used. As a matter of
55
56
57
58
59
60
61
62
63
64
65

1
2
3
4 fact, constraining some parameters during fitting of EXAFS data is not unusual in the
5 literature^{59, 64, 65}. Yet, in order to address our fitting strategy, we tested our fits by varying
6
7 coordination numbers upon finding a reasonable goodness of fit for a given fit performed
8
9 to second coordination shells. Lastly, to make best use of the data we collected, we found
10
11 it appropriate to set CNs for each coordination shell, fit the data and to rely on existing
12
13 information from related techniques.
14
15
16
17

18
19 Spectra of an aqueous solution of 10 mmol L⁻¹ KH₂PO₄ at pH 4.5 (P_(aq)) was
20
21 collected and fit to confirm the position of the multiple scattering (MS) within the PO₄
22
23 tetrahedron. The inclusion of MS improved the fit in the 1.6 – 2.8 Å region as strong MS
24
25 within the PO₄ tetrahedron was expected. We included three MS paths in our fits: namely
26
27 three-legged P – O1 – O2 – P triangular (MS₁), four-legged P – O1 – PO2 – P non
28
29 collinear (MS₂) and four-legged P – O1 – P – O1 – P collinear (MS₃) paths.
30
31
32

33
34 Several different models were employed to fit the MS path, including (i) correlating
35
36 σ^2 MS to 2 times that of the single scattering (SS) path; and (ii) a direct correlation
37
38 between σ^2 MS and that of the SS path⁴³.
39
40
41
42

43 **3. RESULTS & DISCUSSION**

44
45
46
47

48
49 There have been a number of previous studies using spectroscopic techniques to
50
51 characterize phosphate surface complexes forming on Fe(III)-, Al- and Ti (hydr)oxide
52
53 mineral surfaces, including MO/DFT and ATR-FTIR, CIR-FTIR, NMR and XANES
54
55 spectroscopies. Unlike IR spectroscopy, EXAFS analysis is insensitive to the protonation
56
57 environment of surface complexes. Therefore, our discussion will be limited to the
58
59
60
61
62
63
64
65

1
2
3
4 bonding configuration of the surface species. In terms of bonding configuration, the
5
6 bidentate binuclear configuration seems to be the most favorable P sorption complex
7
8 formed at the (hydr)oxides surface (Table 1; ^{12,44,45}). Yet, what has not been established
9
10 in the literature related to P bonding configurations at mineral surfaces are the
11
12 environmental conditions which favor formation of a particular sorption complex
13
14 mechanism. Additionally, the majority of the studies have employed NMR and IR
15
16 techniques. There are no reports in the literature using EXAFS where detailed structural
17
18 information, such as next nearest neighbor, bond distance and coordination numbers are
19
20 reported. A list of relevant studies on P sorption mechanisms formed at mineral
21
22 (hydr)oxides surfaces is shown in Table 1 and is aimed at assisting in the discussion of
23
24 our results.
25
26
27
28
29
30
31
32

33 3.1 P-EXAFS Spectra

34
35 In this study, XANES data are not presented as differences in $\mu(E)$ among spectra
36
37 are very subtle. Figure 1 shows the experimental Fourier Transform results of EXAFS
38
39 data of goethite spiked with P at surface coverages of 1.25, 2.5 and 10 $\mu\text{mol m}^{-2}$ at pH
40
41 4.5. The R-space is a result of the Fourier transformation of the $\chi(k)$ function. The peaks
42
43 shown in the experimental $\chi(k)$ spectra are related to the coordination shells formed
44
45 between P – O and P – Fe and reflect the interatomic distances within the material. For all
46
47 samples, the E_0 ranged from -2.28 to 0.96 eV. The contributions of O were localized at P
48
49 – O distances ranging from 1.51 to 1.53 Å and MS dominates at ~ 2.75 to 2.78 Å. The P –
50
51 Fe shells are indicative of the existence of three different bonding configurations between
52
53 P and the goethite surface and will be treated separately in the following discussion.
54
55
56
57
58
59
60
61
62
63
64
65

Figure 2 shows the k^2 -weighted EXAFS spectra of P sorbed on goethite. The structural parameters obtained from the linear least-square fits are presented in Table 2. A fit was accepted whenever the R-factor value for a given Fourier transform part, reported either in Fourier transform magnitude, real (R) or back-transformed k-space data (q), was less than 6%. That is, the misfit between data and best fit. Figure 4 and 5 show the Real (R) and (q) parts of the Fourier transform of P sorbed on goethite, respectively, at three different surface coverages, 1.25, 2.5 and 10 $\mu\text{mol m}^{-2}$.

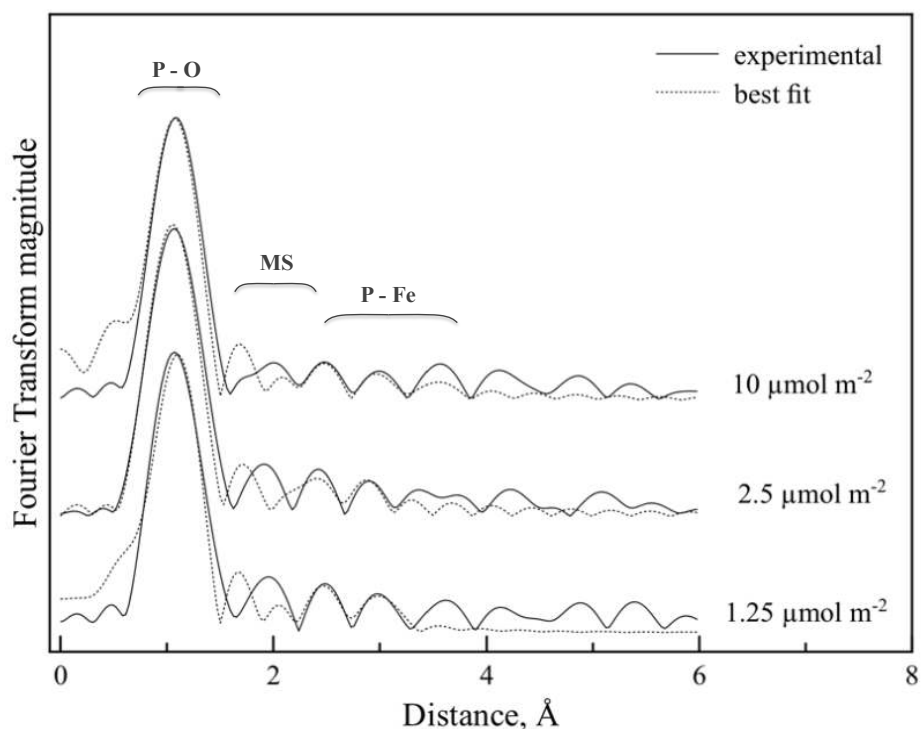


Figure 1. Experimental (solid line) and best fit (dashed line) Fourier transformed spectra of the phosphate surface complexes formed at the goethite/water interface at pH 4.5. A change in spectrum shape (R-space) followed by an increase in the phosphate loading indicates that the phosphate surface speciation changes with surface loading. Braces are intended to show the approximate region where the P – O, multiple scattering

(MS) and P – Fe shells most significantly contribute in radial distance in the Fourier transformed spectra.

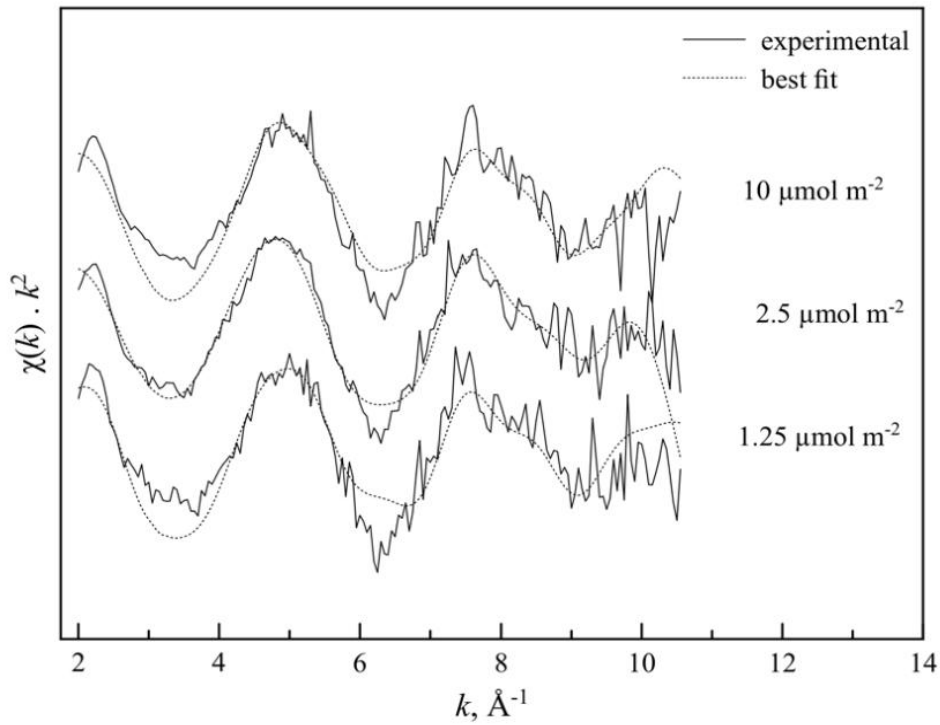


Figure 2. Experimental (solid line) and best-fit (dashed line) k^2 -weighted back-transformed spectra of phosphate sorbed on goethite at 1.25, 2.5 and $10 \mu\text{mol m}^{-2}$ at pH 4.5.

1
2
3
4 3.2 Overall Formation of P Surface Complexes at the Goethite/Water
5
6 Interface
7
8

9 We have identified the formation of three different phosphate surface complexes at
10 the goethite/water interface, namely bidentate mononuclear (²E), bidentate binuclear (²C)
11 and monodentate mononuclear (¹V) surface complexes. Additionally, surface precipitates
12 were also observed, particularly, at higher P loadings.
13
14
15
16
17

18 The shortest P – Fe distances of 2.87 to 2.83 Å are indicative of a bidentate
19 mononuclear configuration between P and Fe at low and intermediate surface loadings,
20 respectively. Intermediate P – Fe distances of 3.27, 3.3 and 3.3 Å were characteristic of a
21 bidentate binuclear configuration between P and Fe at low, intermediate and high surface
22 loadings, respectively. The most distant shell, 3.6 Å, was indicative of a linear
23 configuration between P and Fe. Table 2 shows the P – O and P – Fe bonding distances
24 and corresponding P sorption mechanisms.
25
26
27
28
29
30
31
32
33
34
35
36
37

38 3.3 Adsorption Complexes
39

40 As indicated in Table 2, our results show that bidentate (²C and ²E) surface
41 complexes are predominantly formed at low surface coverages and transition to
42 monodentate configuration as surface coverage increases. This seems consistent with the
43 literature that indicated that low surface coverages favor the formation of bidentate
44 surface complexes^{12, 13, 16, 20, 23, 44 - 47} and that the relative importance of bidentate
45 binuclear species decreases as surface loading increases such that monodentate
46 configuration would predominate at higher surface loadings^{13, 23}. However, on the basis
47 of ATR-FTIR analysis,^{18, 49} observed that P adsorbs mainly as bidentate complexes at
48
49
50
51
52
53
54
55
56
57
58
59
60
61
62
63
64
65

1
2
3
4 high phosphate loadings and that monodentate surface complexes begin to be important
5
6 at low phosphate loadings and at high pHs. This was ascribed to bidentate species
7
8 locating more charge at the surface than monodentate species, producing a lower
9
10 electrostatic repulsion between the adsorbed species in the 1-plane. Interestingly, the
11
12 observation of ^{18, 49} is consistent with the behavior of arsenic in its pentavalent form
13
14 (As(V)), an analog of phosphate, having similar chemical and geometric properties, and
15
16 present as the ionic species, H_2AsO_4^- and H_2PO_4^- , respectively, at the typical pH range in
17
18 the environment.
19
20
21
22

23
24 Because there has not been any EXAFS study on orthophosphate bonding on
25
26 mineral (hydr)oxides, we compared our results to studies relying on (i) MO/DFT and
27
28 planewave/DFT calculations performed by ^{23, 24, 61} on phosphate sorbed to Fe-oxides and
29
30 on (ii) EXAFS of As(V) sorbed on mineral (hydr)oxides. Table 3 shows the P – O and P
31
32 – Fe bonding distances, surface complex distribution and corresponding bonding
33
34 configurations of P on goethite as examined by EXAFS and obtained by MO/DFT and
35
36 planewave/DFT calculations. On an average basis, our EXAFS observations were in good
37
38 agreement with the calculated values, particularly for P – O, where interatomic distances
39
40 varied within 0.05 to 0.1 Å. Likewise, the differences in P – Fe bond lengths for a
41
42 bidentate binuclear configuration were small, varying between 0.04 to 0.07 Å. P – Fe
43
44 distances for a monodentate configuration showed the largest divergence among the two
45
46 approaches, approximately 0.2 Å. With EXAFS studies on As(V), it was observed that
47
48 As(V) can form three bonding configurations with mineral (hydr)oxides surfaces,
49
50 similarly to what was observed in our study ^{50, 51}. However, counter to what was observed
51
52 by these authors, our results show a predominance of the bidentate corner-sharing (²C)
53
54
55
56
57
58
59
60
61
62
63
64
65

1
2
3
4 surface complex at lower surface coverages and a transition to edge-sharing (²E) and
5
6 monodentate corner-sharing (¹V) as surface coverage increased to 10 μmol m⁻². A
7
8 conceptual model depicting the surface loading effect on P surface complexation
9
10 according to P-EXAFS analysis of sorption data from our study is shown in Figure 3.
11
12
13

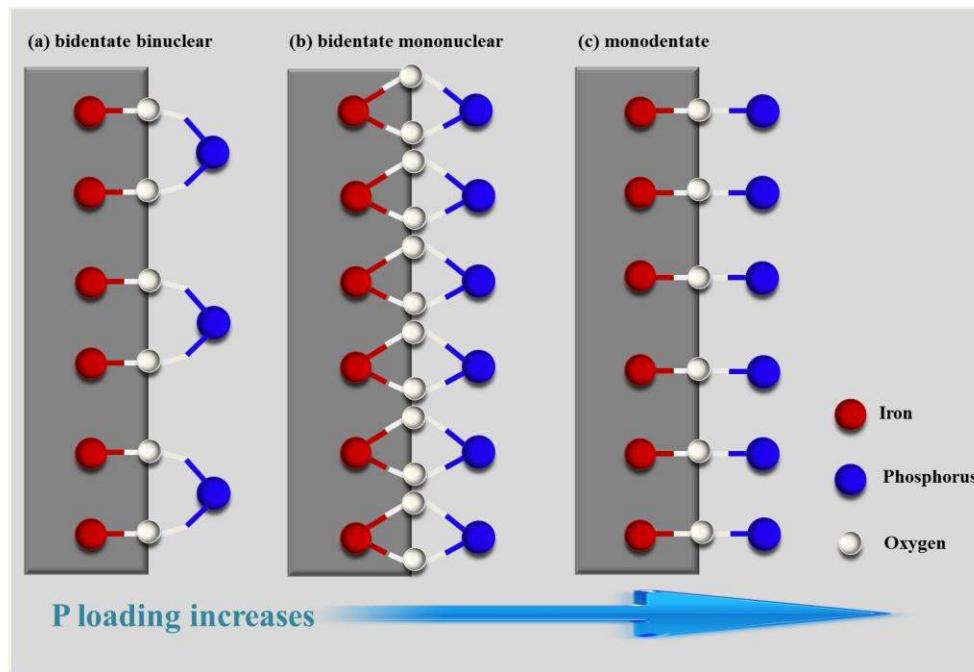


Figure 3. Conceptual model depicting the surface loading effect of P on surface complexation at the goethite/water interface as determined by P-EXAFS analysis of sorption data.

3.3.1 Bidentate Mononuclear Configuration

The shortest P – Fe distances, 2.83 and 2.87 Å, represent an edge sharing between the phosphate tetrahedra and the Fe octahedra. Thus, the only possible configuration for such a short distance would be an edge-sharing bidentate mononuclear configuration (²E). EXAFS spectroscopy has indicated that a bidentate mononuclear configuration (²E) can be formed between tri-, tetra- and penta-valent metals and (hydr)oxide surfaces, such as

1
2
3
4 As(V) on goethite ^{49,50}, Se(IV) on HMO ⁵¹, As(III) on ferrihydrite and on hematite ⁵² and
5
6 As(III) on maghemite ⁵³ under different experimental conditions.
7
8

9
10 However, since the existence of a bidentate mononuclear surface complex between
11 P and (hydr)oxide minerals has never been observed, we tried to rule out its existence by
12 calculating it as forming a 120° angle. In this case, the P-Fe bond distance would be 3.15
13 Å. We also considered that MS contributions could be substantially affecting R at those
14 distances, but this hypothesis was promptly discarded after MS from an aqueous
15 orthophosphate sample (10 mmol L⁻¹ as KH₂PO₄ at pH 4.5) showed MS contributions at
16 around ~ 2.74 Å.
17
18
19
20
21
22
23
24
25

26 Furthermore, the P – Fe distances observed in our study are comparable to those
27 observed in the above-mentioned EXAFS studies, 2.83 – 2.87 Å and 2.87 – 3.08 Å,
28 respectively (reported distances include uncertainties associated with the measure).
29
30
31
32
33
34
35

36 *3.3.2 Bidentate Binuclear Configuration*

37

38 A bidentate binuclear configuration (²C) of phosphate on (hydr)oxides has been
39 shown to be the predominant sorption mechanism formed at lower surface coverages. In
40 this study, the ²C surface complex was present, although at different proportions, across
41 the entire surface coverage range. The rationale for why ²C predominates at lower surface
42 coverages is that this configuration should be favored when the Fe/P ratio is smaller than
43 unity. It follows that at low P concentration, the sorption sites compete with the PO₄
44 molecules at the same strength such that one PO₄ molecule must equally satisfy as many
45 sorption sites as possible. Therefore, ²C forms first and because it is strongly bound to
46 high affinity sorption sites, it has a large thermodynamic stability, thus remaining
47
48
49
50
51
52
53
54
55
56
57
58
59
60
61
62
63
64
65

1
2
3
4 associated with the surface even as solution P concentration increases. In addition, at low
5
6 pHs, i.e., pH ~ 4.5, a higher positive surface charge induces a higher adsorption capacity
7
8 for anions like phosphate, because more negative charge can be brought to the surface for
9
10 a given change in electrostatic potential ⁵³.

11
12
13
14 Table 2 shows the surface complex distribution as a function of surface loading.
15
16 Following the surface complex distribution across the loading range, one can observe that
17
18 the overall percent distribution of ²C remains constant (~50%) when the surface coverage
19
20 increases by a factor of 2.
21
22
23
24
25

26 3.3.3 Monodentate Configuration

27
28 Relatively few spectroscopic studies have reported P being attached to (hydr)oxide
29
30 surfaces in a monodentate (¹V) configuration (Table 1). The studies in which a ¹V
31
32 configuration has been observed were, in general, carried out employing P concentrations
33
34 at relatively high surface coverages ^{13, 16}. Whereas the P – Fe distances for bidentate
35
36 binuclear configuration are in good agreement with the work by ²³, who found P – Fe
37
38 distances varying between 3.22 to 3.26 Å, the P – Fe distance for a monodentate
39
40 configuration observed in our study was much larger, ~ 3.6 Å. Though, this is in
41
42 agreement with the calculations performed by ²⁴, who found P – Fe bond distances
43
44 generally longer for either configuration, if a $\geq 170^\circ$ angle is formed by P – O – Fe,
45
46 suggesting a P – Fe bond distance of around 3.6 Å. EXAFS studies indicate that for
47
48 As(V) these distances are generally in the order of 3.57 to 3.63 Å ^{49, 54}. Since P is a much
49
50 lighter element than As, it is possible that the repulsion of P by the Fe atoms tend to
51
52 maintain P as far apart from Fe as possible, thus P – O – Fe forms preferentially a linear
53
54
55
56
57
58
59
60
61
62
63
64
65

1
2
3
4 structure when a monodentate configuration is formed. Alternatively, the Fe – O bond
5
6 distance may also be influenced by the repulsion and, accordingly, present a longer total
7
8 Fe – P distance.
9

10 11 12 13 14 *3.4 Environmental Significance of our Findings* 15

16 In the highly weathered agricultural soils of the tropics, P is arguably the major
17
18 limiting factor for crop production due to the high sorption capacity of these soils
19
20 together with P's strong binding to mainly Al- and Fe-(hydr)oxide soil minerals. On the
21
22 other hand, over-application of P fertilizers, particularly via application of organic
23
24 amendments, has led to the buildup of soil P to levels at which P loss potential can be
25
26 significantly increased ^{4, 5}. Addressing how P surface complexation (SC) is affected by
27
28 environmental conditions such as surface loading in acidic tropical soils represents a true
29
30 challenge in terms of analytical methods. This is especially true in view of the limitations
31
32 imposed by the techniques that have traditionally been employed, e.g., FTIR, for which
33
34 utilization is constrained under pHs lower than 4.5 ²¹ (which is a soil pH range commonly
35
36 found under tropical conditions) and ³¹P NMR analysis in Fe-rich soils due to Fe
37
38 paramagnetism ²⁰.
39
40
41
42
43
44

45 Our P-EXAFS results represent an advance over the analytical limitations imposed
46
47 by the above-mentioned techniques and provide direct evidence on the molecular basis
48
49 for the low P availability in acidic soils low in P as well as for the greater cycling
50
51 potential of P in soils high in this element. In addition, the research shows the suitability
52
53 of the EXAFS technique to study P surface complexation at mineral/water interfaces
54
55 under conditions typically found in tropical soils, that is, at relatively low P
56
57
58
59
60
61
62
63
64
65

1
2
3
4 concentrations ($2.5 \mu\text{mol L}^{-1}$, i.e., 77.5 mg kg^{-1}) and at low pHs, as EXAFS is
5
6 insensitivity to the later.
7
8

9 Our results indicated that P was rapidly (< 5 days) sorbed at the goethite surface,
10
11 even at surface loadings above the P loadings predicted for monolayer coverage on
12
13 goethite. Regardless of the P surface loadings employed in this study, P sorbed on
14
15 goethite via a ligand exchange mechanism, that is, forming a quite stable surface
16
17 complex. It was also observed that surface loading has a marked effect on surface
18
19 complexation, which transitioned from bidentate binuclear into bidentate mononuclear or
20
21 monodentate with increases in surface loading (Figure 3). This continuum of binding
22
23 mechanisms corroborates the vast literature indicating the thermodynamic feasibility for
24
25 the formation of more stable structures at low surface coverages, where P availability is
26
27 constrained due to the much higher binding energy involved^{12, 44-46}. In most acidic soils,
28
29 the available P pool associated with soil minerals is usually low and only a small fraction
30
31 of sorbed P is readily desorbable, most likely from solid phases formed from recent
32
33 additions of fertilizer P or physically sorbed phosphate by less energetic binding. Over
34
35 fertilization of P may, therefore, enhance P availability and mobility due to formation of
36
37 monodentate surface complexes, which have a less energetic character, and are favored at
38
39 high surface coverages.
40
41
42
43
44
45
46
47
48
49

50 **4. ACKNOWLEDGEMENTS**

51
52 The senior author gratefully acknowledges the receipt of a Delaware Environmental
53
54 Institute (DENIN) graduate fellowship. The authors appreciate financial support from the
55
56 U.S. National Science Foundation via Delaware EPSCoR. Support for this project was
57
58
59
60
61
62
63
64
65

1
2
3
4
5
6
7
8
9
10
11
12
13
14
15
16
17
18
19
20
21
22
23
24
25
26
27
28
29
30
31
32
33
34
35
36
37
38
39
40
41
42
43
44
45
46
47
48
49
50
51
52
53
54
55
56
57
58
59
60
61
62
63
64
65

made possible by the Unidel Foundation and by Delaware EPSCoR with funds from the National Science Foundation Grant EPS-0814251. We also extend our thanks to the United States Department of Energy for providing us access to the National Synchrotron Light Source and for the technical support provided by the later.

Table 1. Relevant studies on the P sorption mechanisms formed at mineral (hydr)oxide surfaces using MO/DFT, ATR-FTIR, CIR-FTIR, NMR and XANES spectroscopies.

Surface complex	Technique	Surface loading, ($\mu\text{mol m}^{-2}$)*, (mmol L^{-1})**, (mmol kg^{-1} *** or P/Fe****)	Sorbent	Reference
Monodentate	CIR-FTIR	high, >> 17****	Goethite	Tejedor-Tejedor & Anderson, 1990 ¹³
	ATR-FTIR	0.4 **	Goethite	Persson et al., 1996 ¹⁴
		high, ~ 0.5 **	Hematite	Elzinga & Sparks, 2007 ¹⁶
	MO/DFT	high, >> 1.5 *	Goethite	Rahnemaie et al., 2007 ²³
	NMR	0.1 – 100 **	Boehmite	Kim & Kirkpatrick, 2004 ²⁰
Bidentate	CIR-FTIR	low, << ~ 0.2	Goethite	Tejedor-Tejedor & Anderson, 1990 ¹³
		initial conc. ~ 5**	TiO ₂	Connor & McQuillan, 1999 ⁶⁰
	ATR-FTIR	0.38 – 2.69*	Ferrihydrite	Arai & Sparks, 2001 ¹⁵
		initial conc. ~ 0.06**	Goethite	Luengo et al., 2006 ¹⁷
		> ~ 0.2*	Goethite	Antelo et al., 2005 ²
	MO/DFT	low ~ 0.005 **	Hematite	Elzinga & Sparks, 2007 ¹⁶
		low < 1.5 *	Goethite	Rahnemaie et al., 2007 ²³
	ATR-FTIR, planewave/ DFT	0.1 **	Goethite	Kubicki et al., 2012 ⁶¹
	NMR	0.1 – 150*	Boehmite and γ -alumina	Kim & Kirkpatrick, 2004 ²⁰
		0.1 – 1.0 **	Boehmite	Li et al., 2010 ²¹
		0.1 – 3.0 **	Akaganeite, boehmite, lepidocrocite	Kim et al., 2011 ²²
		2.6 – 26*	α -Al ₂ O ₃	Li et al., 2013a ⁶²
	NMR, ATR-FTIR, MO/DFT	0.15 – 150*	boehmite, corundum, gibbsite, bayerite and γ -alumina	Li et al., 2013b ⁶³
XANES				750****

1
2
3
4
5
6
7
8
9
10
11
12
13
14
15
16
17
18
19
20
21
22
23
24
25
26
27
28
29
30
31
32
33
34
35
36
37
38
39
40
41
42
43
44
45
46
47
48
49
50
51
52
53
54
55
56
57
58
59
60
61
62
63
64
65

300 – 830***

Boehmite

1 Table 2. P – O and P – Fe bonding distances, surface complex distribution and corresponding bonding configurations of P on
 2 goethite at three different surface coverages.

Surface loading $\mu\text{mol m}^{-2}$	P – O		Surface Complexes								
			Bidentate mononuclear			Bidentate binuclear			Monodentate		
	R	σ^2	R	σ^2	fraction	R	σ^2	fraction	R	σ^2	fraction
	(Å)		(Å)		(%)	(Å)		(%)	(Å)		(%)
1.25	1.51	0.0021	2.87	0.0032	48	3.27	0.0033	47			
	(±0.01)		(±0.03)			(±0.06)					
2.5	1.52	0.0004	2.83	0.0052	77	3.3	0.0030	25			
	(±0.01)		(±0.04)			(±0.08)					
10	1.51	0.0004				3.3	0.0002	18	3.6	0.0035	63
	(±0.01)					(±0.05)			(±0.04)		

3 R: radial structure function (RSF); σ^2 : mean square displacement, (): uncertainties associated with parameter estimates

4

Table 3. P – O and P – Fe bonding distances, surface complex distribution and corresponding bonding configurations of P on goethite as examined by EXAFS and obtained by MO/DFT calculations from Kwon & Kubicki (2004), Rahnemaie et al. (2007) and planewave/DFT calculations by Kubicki et al. (2012). The values shown on the table correspond to the average of each individual value for a given surface complex.

Surface complex	EXAFS ¹		Kwon & Kubicki, 2004		Rahnemaie et al., 2007		Kubicki et al., 2012	
	P – O	P – Fe	P – O	P – Fe	P – O	P – Fe	P – O	P – Fe
	Å							
Monodentate	1.51	3.6	1.57	3.37	1.61	3.6	1.56	3.42 (3.25 – 3.55) ³
Bidentate binuclear	1.51	3.28	1.59	3.21	1.6	3.24	1.56	3.28 (3.18 – 3.45) ³
Bidentate mononuclear	1.52	2.85	NO ²	NO ²	NO ²	NO ²	NO ²	NO ²

Bond distances represent an average for the three surface loadings in Table 2.¹

NO²: Not observed.

The numbers in parenthesis indicate the range of P – Fe bond lengths found by Kubicki et al., 2012.³

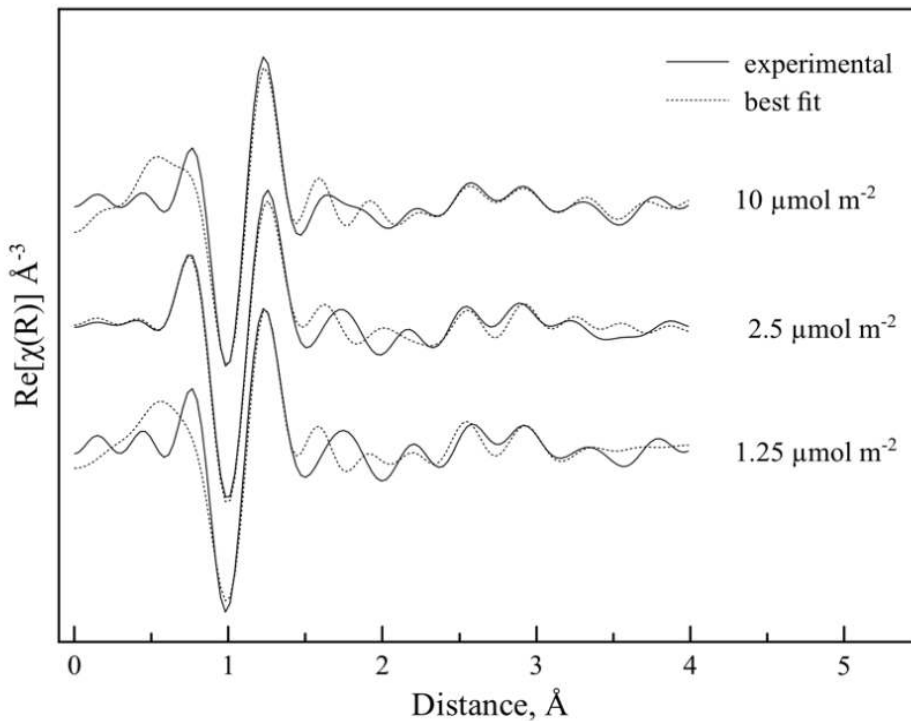
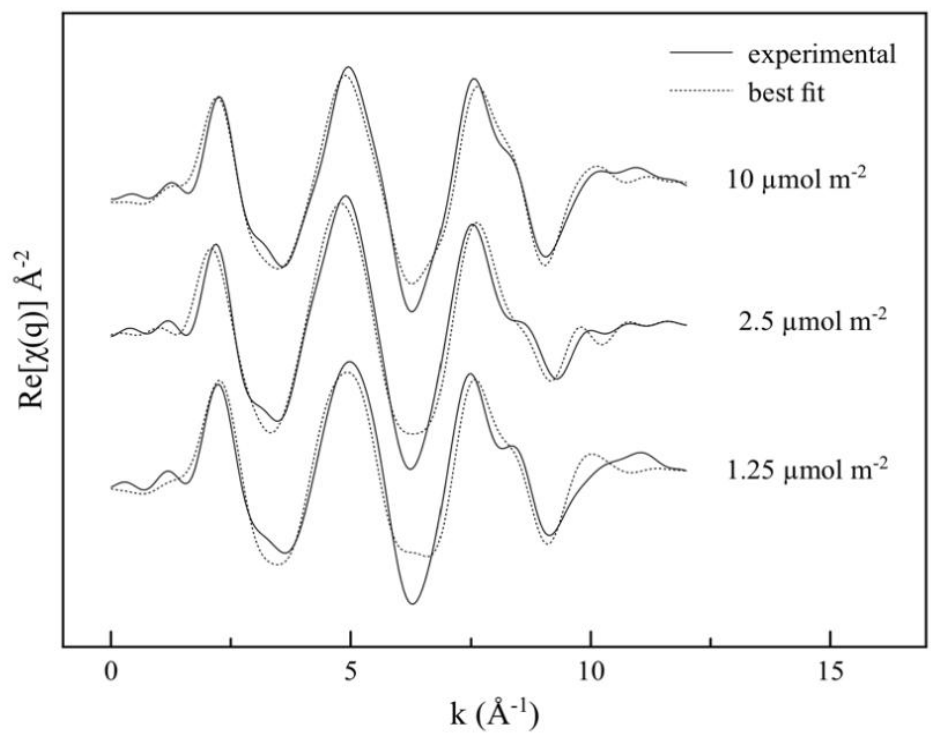


Figure 4. Real (R) part of the Fourier Transform of P sorbed on goethite at three different surface coverages, 1.25, 2.5 and 10 $\mu\text{mol m}^{-2}$.

1
2
3
4 17
5
6 18
7
8
9



10
11
12
13
14
15
16
17
18
19
20
21
22
23
24
25
26
27
28
29
30
31
32
33 19
34
35 20
36
37
38 21
39
40 22
41
42 23
43
44
45 24
46
47 25
48
49
50 26
51
52 27
53
54 28
55
56
57 29
58
59 30
60
61
62
63
64
65

Figure 5. Real (q) part of the Fourier Transform of P sorbed on goethite at three different surface coverages, 1.25, 2.5 and 10 $\mu\text{mol m}^{-2}$.

1
2
3
4
5
6
7
8
9
10
11
12
13
14
15
16
17
18
19
20
21
22
23
24
25
26
27
28
29
30
31
32
33
34
35
36
37
38
39
40
41
42
43
44
45
46
47
48
49
50
51
52
53
54
55
56
57
58
59
60
61
62
63
64
65

5. REFERENCES

(1) Novais, R. F. & Smyth, T. J. Fósforo em solo e planta em condições tropicais. Viçosa, MG, Universidade Federal de Viçosa, 1999. 399p

(2) Antelo, J., Avena, M., Fiol, S., Lopez, R., Arce, F. Effects of pH and ionic strength on the adsorption of phosphate and arsenate at the goethite–water interface. *J. Colloid Interface Sci.*, 285:476–486, 2005

(3) Kruse, J. & Leinweber, P. Phosphorus in sequentially extracted fen peat soils: A K-edge X-ray absorption near-edge structure (XANES) spectroscopy study. *J. Plant Nutr. Soil Sc.*, 171:613-620, 2008

(4) Abdala, D. B., Ghosh, A. K., Silva, I. R., Novais, R. F. Alvarez V., V. H. Phosphorus saturation of a tropical soil and related P leaching caused by poultry litter addition. *Agr Ecosyst Environ.*, 162:15–33, 2012

(5) Abdala, D. B., Silva, I. R., Vergütz, L., Sparks, D. L. Long-term manure application effects on phosphorus speciation, kinetics and distribution in highly weathered agricultural soils. *Chemosphere*, in press, 2014

(6) Fried, C. R. & Shapiro, G. Phosphate supply pattern of various soils. *Soil Sci. Soc. Am. Proc.*, 20:471–475, 1956

1
2
3
4
5
6
7
8
9
10
11
12
13
14
15
16
17
18
19
20
21
22
23
24
25
26
27
28
29
30
31
32
33
34
35
36
37
38
39
40
41
42
43
44
45
46
47
48
49
50
51
52
53
54
55
56
57
58
59
60
61
62
63
64
65

54

55

(7) Olsen, S. R. & Watanabe, F. S. A method to determine a phosphorus adsorption maximum of soils as measured by the Langmuir isotherm. Soil Sci. Soc. Am. Proc., 21:144-149, 1957

56

57

58

59

(8) Hingston, F. J., Atkinson, R. J., Posner, A. M., Quirk, J. P. Specific adsorption of anions on goethite. Congr. Soil Sci. Soc. 9th (Adelaide), 669-678, 1968

60

61

62

63

(9) Hingston, F. J., R. J., Posner, A. M., Quirk, J. P. Competitive adsorption of negatively charged ligands on oxide surfaces. Disc. Faraday Soc., 52:334-342, 1971

64

65

66

67

(10) Hingston, F. J., R. J., Posner, A. M., Quirk, J. P. Anion adsorption by goethite and gibbsite. I. The role of the proton in determining adsorption envelopes. J. Soil Sci., 23:177-192, 1972

68

69

70

71

(11) Hingston, F. J., R. J., Posner, A. M., Quirk, J. P. Anion adsorption by goethite and gibbsite. II. Desorption of anions from hydrous oxide surfaces. J. Soil Sci., 25:16-26, 1974

72

73

74

75

(12) Parfitt, R. L., R. J. Atkinson, R. St. C. Smart. The mechanism of phosphate fixation by iron oxides. Soil Sci. Soc. Am. J., 39:837-841, 1975

76

1
2
3
4
5
6
7
8
9
10
11
12
13
14
15
16
17
18
19
20
21
22
23
24
25
26
27
28
29
30
31
32
33
34
35
36
37
38
39
40
41
42
43
44
45
46
47
48
49
50
51
52
53
54
55
56
57
58
59
60
61
62
63
64
65

77
78
79
80
81
82
83
84
85
86
87
88
89
90
91
92
93
94
95
96
97

(13) Tejedor-Tejedor, M. I. & Anderson, M. A. The protonation of phosphate on the surface of goethite as studied by CIR-FTIR and electrophoretic mobility. *Langmuir*, 6:602–611, 1990

(14) Persson, P., Nilsson, N., Sjoberg, S. Structure and Bonding of Orthophosphate Ions at the Iron Oxide–Aqueous Interface. *J. Colloid Interface Sci.*, 177:263–275, 1996

(15) Arai, Y. & Sparks, D. L. ATR-FTIR spectroscopic investigation on phosphate adsorption mechanisms at the ferrihydrite-water interface. *J. Colloid Interface Sci.*, 241: 317-326, 2001

(16) Elzinga, E. J. & Sparks, D. L. Phosphate adsorption onto hematite: An in situ ATR-FTIR investigation of the effects of pH and loading level on the mode of phosphate surface complexation. *J. Colloid Interface Sci.*, 308:53–70, 2007

(17) Luengo, C., Brigante M., Antelo, J., Avena, M. Kinetics of phosphate adsorption on goethite: Comparing batch adsorption and ATR-IR measurements. *J. Colloid Interface Sci.*, 300:511-518, 2006

1
2
3
4
5
6
7
8
9
10
11
12
13
14
15
16
17
18
19
20
21
22
23
24
25
26
27
28
29
30
31
32
33
34
35
36
37
38
39
40
41
42
43
44
45
46
47
48
49
50
51
52
53
54
55
56
57
58
59
60
61
62
63
64
65

98 (18) Antelo, J., Fiol, S., Pérez, C., Mariño, S., Arce, F., Gondar, D. López, R.
99 Analysis of phosphate adsorption onto ferrihydrite using the CD-MUSIC model. J.
100 Colloid Interface Sci., 347:112-119, 2010

101

102 (19) Bleam, W. F., Pfeffer, P. E., Goldberg, S., Taylor, R. W., Dudley, R. A.
103 ³¹P Solid-state Nuclear Magnetic Resonance study of phosphate adsorption at the
104 boehmite/aqueous solution interface. Langmuir, 7:1702–1712, 1991

105

106 (20) Kim, Y. & Kirkpatrick, R. J. An investigation of phosphate adsorbed on
107 aluminium oxyhydroxide and oxide phases by nuclear magnetic resonance. Eur. J.
108 Soil Sci., 55:243–251, 2004

109

110 (21) Li, W., Feng, J., Kwon, K. D., Kubicki, J. D. Phillips, B. L. Surface
111 speciation of phosphate on boehmite (γ -AlOOH) determined from NMR
112 spectroscopy. Langmuir, 26:4753–4761, 2010

113

114 (22) Kim, J., Li, W., Philips, B. L., Grey, C. P. Phosphate adsorption on
115 the iron oxyhydroxides goethite (α -FeOOH), akaganeite (β -FeOOH),
116 and lepidocrocite (γ -FeOOH): a ³¹P NMR Study. Energy Environ. Sci., 4:4298-
117 4305, 2011

118

1
2
3
4
5
6
7
8
9
10
11
12
13
14
15
16
17
18
19
20
21
22
23
24
25
26
27
28
29
30
31
32
33
34
35
36
37
38
39
40
41
42
43
44
45
46
47
48
49
50
51
52
53
54
55
56
57
58
59
60
61
62
63
64
65

119 (23) Rahnemaie R., Hiemstra T., van Riemsdijk W. H. Geometry, charge
120 distribution, and surface speciation of phosphate on goethite. *Langmuir*, 23:3680-
121 3689, 2007

122

123 (24) Kwon, K. D. & Kubicki, J. D. Molecular orbital theory study on surface
124 complex structures of phosphates to iron hydroxides: Calculation of vibrational
125 frequencies and adsorption energies. *Langmuir*, 20:9249-9254, 2004

126

127 (25) Arai, Y. & Sparks, D. L. Phosphate reaction dynamics in soils and soil
128 minerals: A Multiscale Approach, *In Advances in Agronomy*, 94: 135-179, 2007

129

130 (26) Carabante, I., Grahn, M., Holmgren, A. Hedlund, J. In situ ATR-FTIR
131 studies on the competitive adsorption of arsenate and phosphate on ferrihydrite. *J.*
132 *Colloid Interface Sci.*, 351:523-531, 2010

133

134 (27) Charlet, L. & Manceau, A. X-ray absorption spectroscopic study of the
135 sorption of Cr(III) at the oxide-water interface : II. Adsorption, coprecipitation, and
136 surface precipitation on hydrous ferric oxide. *J. Colloid Interface Sci.*, 148: 443-
137 458, 1992

138

139 (28) Fendorf, S. Surface reactions of chromium in soils and waters.
140 *Geoderma* 67:55–71, 1995

141

1
2
3
4
5
6
7
8
9
10
11
12
13
14
15
16
17
18
19
20
21
22
23
24
25
26
27
28
29
30
31
32
33
34
35
36
37
38
39
40
41
42
43
44
45
46
47
48
49
50
51
52
53
54
55
56
57
58
59
60
61
62
63
64
65

142 (29) Scheidegger, A. M., Lamble, G. M., Sparks, D. L. Spectroscopic
143 evidence for the formation of mixed-cation, hydroxide phases upon metal sorption
144 on clays and aluminum oxides. *J. Colloid Interface Sci.*, 186:118-128, 1997

145
146 (30) Scheidegger, A. M., Strawn, D. G., Lamble, G.M., Sparks, D.L. The
147 kinetics of mixed Ni-Al hydroxide formation on clay and aluminum oxide minerals:
148 A time-resolved XAFS study. *Geochim. Cosmochim. Acta*, 62:2233-2245, 1998

149
150 (31) Ford, R. G. & Sparks, D. L. The nature of Zn precipitates formed in the
151 presence of pyrophyllite. *Environ. Sci. Technol.* 34:2479-2483, 2000

152
153 (32) Roberts, D. R., Ford, R.G., Sparks, D. L. Kinetics and mechanisms of Zn
154 complexation on metal oxides using EXAFS spectroscopy. *J. Colloid Interface Sci.*,
155 263:364-376, 2003

156
157 (33) Nachttegaal, M. & Sparks, D. L. Effect of iron oxide coatings on zinc
158 sorption mechanisms at the clay-mineral/water interface. *J. Colloid Interface Sci.*
159 276:13-23, 2004

160
161 (34) Sparks, D. L. *Environmental Soil Chemistry. Second Edition.* Academic
162 Press, 2002, 368 pg.

163

1
2
3
4
5
6
7
8
9
10
11
12
13
14
15
16
17
18
19
20
21
22
23
24
25
26
27
28
29
30
31
32
33
34
35
36
37
38
39
40
41
42
43
44
45
46
47
48
49
50
51
52
53
54
55
56
57
58
59
60
61
62
63
64
65

164 (35) Manning, B. A., Fendorf, S. E., Goldberg, S. Surface structures and
165 stability of arsenic(III) on goethite: Spectroscopic evidence for inner-sphere
166 complexes. *Environ. Sci. Technol.*, 32:2383-2388, 1998

167

168 (36) Peak, J. D. & Sparks, D. L. Mechanisms of selenate adsorption on iron
169 oxides and hydroxides. *Environ. Sci. Technol.*, 36:1460-1466, 2002

170

171 (37) Hesterberg, D., Zhou, W., Hutchison, K. J., Beauchemin, S., Sayers, D.
172 E. XAS study of adsorbed forms of phosphate. *J. Synchrotron Rad.*, 6:636-638,
173 1999

174

175 (38) Khare, N., D. Hesterberg, and J. D. Martin. Investigating phosphate
176 surface precipitation in single and binary mixtures of Fe- and Al-oxide minerals
177 using XANES. *Environ. Sci. Technol.*, 39:2152-2160, 2005

178

179 (39) Khare, N., Martin, J. D., Hesterberg, D. Phosphate bonding configuration
180 on ferrihydrite based on molecular orbital calculations and XANES fingerprinting.
181 *Geochim. Cosmochim. Acta*, 71:4405-4415, 2007

182

183 (40) Schwertmann, U., Cornell, R. M. *Iron Oxides in the Laboratory:*
184 *Preparation and Characterization*; Wiley-VCH: Weinheim, Germany, 2000

185

1
2
3
4
5
6
7
8
9
10
11
12
13
14
15
16
17
18
19
20
21
22
23
24
25
26
27
28
29
30
31
32
33
34
35
36
37
38
39
40
41
42
43
44
45
46
47
48
49
50
51
52
53
54
55
56
57
58
59
60
61
62
63
64
65

186 (41) Ravel, B. & Newville, M. ATHENA and ARTEMIS: interactive
187 graphical data analysis using IFEFFIT. *J. Synchrotron Rad.* 12:537–541, 2005

188
189 (42) Newville, M., Livins, P., Yacoby, Y., Rehr, J. J., Stern, E. A. Near-edge
190 x-ray-absorption fine structure of Pb: A comparison of theory and experiment.
191 *Phys. Rev. B Condens. Matter* 47:14126–14131,1993

192
193 (43) Rouff, A. A., Natchegaal, M., Rabe, S., Vogel, F. X-ray absorption fine
194 structure study of the effect of protonation on disorder and multiple scattering in
195 phosphate solutions and solids. *J. Phys. Chem. A.*, 113:6895-903, 2009

196
197 (44) Parfitt, R. L. Anion adsorption by soils and soil materials. *Advances in*
198 *Agronomy*, 30:1-50, 1978

199
200 (45) Parfitt, R. L. The mechanism of phosphate fixation by iron oxides. *Soil*
201 *Sci. Soc. Am. Proc.*, 39:837-841, 1975

202
203 (46) Parfitt, R. L., Atkinson, R. J. Phosphate adsorption on goethite (α -
204 FeOOH). *Nature*, 264:740-742, 1976

205
206 (47) Parfitt, R.L., & Russell, J. D. Adsorption on hydrous oxides. IV.
207 Mechanisms of adsorption of various ions on goethite. *J. Soil Sci.*, 28:297-305,
208 1977

1
2
3
4
5
6
7
8
9
10
11
12
13
14
15
16
17
18
19
20
21
22
23
24
25
26
27
28
29
30
31
32
33
34
35
36
37
38
39
40
41
42
43
44
45
46
47
48
49
50
51
52
53
54
55
56
57
58
59
60
61
62
63
64
65

209
210
211
212
213
214
215
216
217
218
219
220
221
222
223
224
225
226
227
228
229
230
231

(48) Fendorf, S. E., Eick, M. J., Grossl, P. R., Sparks, D. L. Arsenate and chromate retention mechanisms on goethite. 1. Surface structure. Environ. Sci. Technol. 31:315-320, 1997

(49) Grossl, P. R., Eick, M. J., Sparks, D. L., Goldberg, S., Ainsworth, C. C. Arsenate and chromate retention mechanisms on goethite. 2. Kinetic evaluation using a pressure-jump relaxation technique. Environ. Sci. Technol., 31:321-326, 1997

(50) Foster, A., Brown, G. E., Parks, G. A. X-ray absorption fine structure study of As(V) and Se(IV) sorption complexes on hydrous Mn oxides. Geochim. Cosmochim. Acta, 67:1937–1953, 2003

(51) Ona-Nguema G., Morin, G., Juillot, F., Calas, G. Brown, G. E. EXAFS analysis of arsenite adsorption onto two-line ferrihydrite, hematite, goethite, and lepidocrocite. Environ. Sci. Technol., 39:9147–9155, 2005

(52) Morin, G., Ona-Nguema, G., Wang, Y., Menguy, N., Juillot, F., Proux, O., Guyot, F., Calas, G., Brown Jr., G. E. Extended X-ray absorption fine structure analysis of arsenite and arsenate adsorption on maghemite, Environ. Sci. Technol., 42:2361–2366, 2008

1
2
3
4
5
6
7
8
9
10
11
12
13
14
15
16
17
18
19
20
21
22
23
24
25
26
27
28
29
30
31
32
33
34
35
36
37
38
39
40
41
42
43
44
45
46
47
48
49
50
51
52
53
54
55
56
57
58
59
60
61
62
63
64
65

232 (53) Hiemstra, T. Surface complexation at mineral interfaces: Multisite and
233 Charge Distribution approach. (Ph.D. thesis), Wageningen University, 2010

234
235 (54) Waychunas G. A., Rea, B. A., Fuller, C. C., Davis, J. A. Surface
236 chemistry of ferrihydrite. 1. EXAFS studies of the geometry of coprecipitated and
237 adsorbed arsenate. *Geochim. Cosmochim. Acta*, 57:2251–2269, 1993

238
239 (55) Corey, R. B. Adsorption vs. coprecipitation, (1981) pp.161-182. In:
240 (Anderson, M. A. & Rubin, A. J. eds.) *Adsorption of Inorganics at Solid-Liquid*
241 *Interfaces*, Ann Arbor Science, Ann Arbor Mich.

242
243 (56) Torrent, J. Activation energy of the slow reaction between phosphate and
244 goethites of different morphology. *Aust. J. Soil Res.*, 29:69-74, 1990

245
246 (57) Dzombak, D. A., & Morel, F. M. M. *Surface Complexation Modeling:*
247 *Hydrous Ferric Oxide*. Wiley-Interscience, 1990. New York, 393 pp.

248
249 (58) Antelo, J., Arce, F., Avena, M., Fiol, S., López R., Macías, F. Adsorption
250 of a soil humic acid at the surface of goethite and its competitive interaction with
251 phosphate. *Geoderma*, 138:12-19, 2007

252

1
2
3
4
5
6
7
8
9
10
11
12
13
14
15
16
17
18
19
20
21
22
23
24
25
26
27
28
29
30
31
32
33
34
35
36
37
38
39
40
41
42
43
44
45
46
47
48
49
50
51
52
53
54
55
56
57
58
59
60
61
62
63
64
65

253 (59) Arai, Y., Elzinga, E. J., Sparks, D. L. X-ray absorption spectroscopic
254 investigation of arsenite and arsenate adsorption at the aluminum oxide-water
255 interface. *J. Colloid Interface Sci.*, 235:80-88, 2001

256
257 (60) Connor, P. A. & McQuillan, A. J. Phosphate adsorption onto TiO₂ from
258 aqueous solutions: an in situ internal reflection infrared spectroscopic study.
259 *Langmuir*, 15:2916-2921, 1999

260
261 (61) Kubicki, J. D.; Paul, K. W.; Kabalan, L.; Zhu, Q.; Mroziak, M. K.;
262 Aryanpour, M.; Pierre-Louis, A.; Strongin, D. R. ATR-FTIR and density
263 functional theory study of the structures, energetics, and vibrational spectra of
264 phosphate adsorbed onto goethite. *Langmuir*, 28:14573-14587, 2012

265
266 (62) Li, W., Andro-Marc Pierre-Louis, A. M., Kwon, K. D., Kubicki, J. D.,
267 Strongin, D. R., Phillips, B. L. Molecular level investigations of phosphate
268 sorption on corundum (α -Al₂O₃) by ³¹P solid state NMR, ATR-FTIR and quantum
269 chemical calculation. *Geochim. Cosmochim. Acta*, 107:252-266, 2013

270
271 (63) Li W., Feng, X., Yan, Y., Sparks, D. L., Phillips, B. L. Solid state NMR
272 spectroscopic study of phosphate sorption mechanisms on aluminum
273 (hydr)oxides. *Environ. Sci. Technol.*, 15: 8308-8315, 2013

274

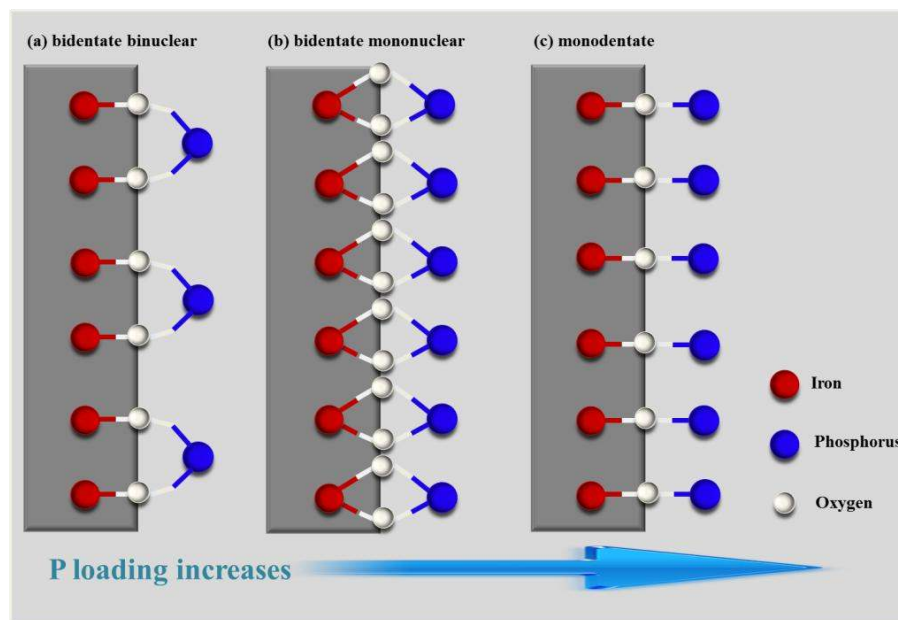
1
2
3
4
5
6
7
8
9
10
11
12
13
14
15
16
17
18
19
20
21
22
23
24
25
26
27
28
29
30
31
32
33
34
35
36
37
38
39
40
41
42
43
44
45
46
47
48
49
50
51
52
53
54
55
56
57
58
59
60
61
62
63
64
65

275
276
277
278
279
280
281
282
283

(64) Bostick, B. C. & Fendorf, S. E. Arsenite sorption on troilite (FeS) and pyrite (FeS₂). *Geochim. Cosmochim. Acta*, 67:909-921, 2003

(65) Sherman, D. & Randall, S. R. Surface complexation of arsenic(V) to iron(III) (hydr)oxides: structural mechanisms from ab initio molecular geometries and EXAFS spectroscopy. *Geochim. Cosmochim. Acta*, 67:4223-4230, 2003

Table of Contents Graph (TOC Art):



284